*Article*

# Post-War Urban Damage Mapping Using InSAR: The Case of Mosul City in Iraq

Ali Darvishi Boloorani [1,2,*], Mehdi Darvishi [3], Qihao Weng [4] and Xiangtong Liu [1]

[1] Key Laboratory of Digital Land and Resources, East China University of Technology, Nanchang 330013, China; xtliu@ecit.cn
[2] Department of Remote Sensing and GIS, Faculty of Geography, University of Tehran, Tehran, Iran
[3] Department of Physical Geography, Stockholm University, SE-106 91 Stockholm, Sweden; mehdi.darvishi@natgeo.su.se
[4] Centre for Urban and Environmental Change, Department of Earth & Environmental Systems, Indiana State University, Terre Haute, IN 47809-1902, USA; qweng@indstate.edu
[*] Correspondence: ali@ecut.edu.cn or ali.darvishi@ut.ac.ir

**Abstract:** Urban infrastructures have become imperative to human life. Any damage to these infrastructures as a result of detrimental activities would accrue huge economical costs and severe casualties. War in particular is a major anthropogenic calamity with immense collateral effects on the social and economic fabric of human nations. Therefore, damaged buildings assessment plays a prominent role in post-war resettlement and reconstruction of urban infrastructures. The data-analysis process of this assessment is essential to any post-disaster program and can be carried out via different formats. Synthetic Aperture Radar (SAR) data and Interferometric SAR (InSAR) techniques help us to establish a reliable and fast monitoring system for detecting post-war damages in urban areas. Along this thread, the present study aims to investigate the feasibility and mode of implementation of Sentinel-1 SAR data and InSAR techniques to estimate post-war damage in war-affected areas as opposed to using commercial high-resolution optical images. The study is presented in the form of a survey to identify urban areas damaged or destroyed by war (Islamic State of Iraq and the Levant, ISIL, or ISIS occupation) in the city of Mosul, Iraq, using Sentinel-1 (S1) data over the 2014–2017 period. Small BAseline Subset (SBAS), Persistent Scatterer Interferometry (PSI) and coherent-intensity-based analysis were also used to identify war-damaged buildings. Accuracy assessments for the proposed SAR-based mapping approach were conducted by comparing the destruction map to the available post-war destruction map of United Nations Institute for Training and Research (UNITAR); previously developed using optical very high-resolution images, drone imagery, and field visits. As the findings suggest, 40% of the entire city, the western sectors, especially the Old City, were affected most by ISIS war. The findings are also indicative of the efficiency of incorporating Sentinel-1 SAR data and InSAR technique to map post-war urban damages in Mosul. The proposed method could be widely used as a tool in damage assessment procedures in any post-war reconstruction programs.

**Keywords:** post-war destruction mapping; synthetic aperture radar (SAR) data; interferometric SAR (InSAR); Sentinel-1

## 1. Introduction

Urban environments are complex systems that support human life and must constantly be monitored in order to avoid catastrophic loss of infrastructures and lives [1]. Cities have been destroyed throughout history by various processes, both natural and anthropogenic. War in particular gives rise to many of these cases anywhere it takes place, often causing irreparable damage to urban infrastructures. However, an accurate, reliable, cost-effective, and fast post-war mapping-monitoring system would facilitate the process of assessing damages inflicted by war on urban infrastructures. Along this line, the following elaborates

on the importance of war-damage assessment for urban infrastructures and makes mention of the existing tools used for monitoring the severity of damages.

In the past decade, new generations of satellite sensors have been launched and several automated techniques have been developed for the study of urban areas, exploiting both active synthetic aperture radar (SAR) and passive sensors [2,3]. Many of these studies address the issue of change detection in urban areas, incorporating SAR images with different approaches such as using multi-pass interferometric data in 3D reconstruction and monitoring buildings, particularly those affected by systematic displacements related to natural hazards, specifically landslides [4]. For instance, using SAR and VHR (Very High Resolution) optical images to quantify damages caused by the 2003 Bam earthquake in Iran [5] and using multi-SAR data to study the 2009 L'Aquila earthquake in Italy [6].

In another case, urban destruction detection of the civil war in Syria (2011–2017) was carried out using optical images [7]. They used the Gray-Level Co-Occurrence Matrix (GLCM) and two texture-based metrics (correlation and homogeneity) to identify the damaged buildings in Aleppo. In another related study, the principal components (PCs) of multiple textural features and image correlation were tested to detect the changes associated with the building collapse caused by an earthquake that hit L'Aquila city (Italy) on 6 April 2009 [8]. Artificial intelligence-based algorithms such as deep learning [9], polarimetric SAR data [10] and updating of buildings database [11] are all among other case studies that have been used for the quantitative estimation of structural damages to buildings. Very high-resolution images from the IKONOS and QuickBird satellites have also been utilized to detect and quantify structural damages to buildings [12,13]. However, post-disaster building damage detection using very high-resolution optical images and field visits are costly and face certain constraints such as cloudiness and satellite revisit period.

Coherence and intensity information of SAR data [14] can also be utilized along with optical data [15] to detect changes in urban infrastructures. Coherence is used as a measure of damage in buildings. Cases of the use of this measure can be seen in [16,17], where coherence coefficient before and after earthquake events were used to estimate building damage. The studies showed that a shorter perpendicular baseline provides a clear decorrelation in the damaged areas than a longer baseline [18,19], facilitating the process of damage detection. As a result, S1 data with a short spatial baseline (usually less than 250 m) and revisit-time of 12/6 days provide a promising opportunity for urban damage detection.

The primary objective of the Differential SAR Interferometry (DInSAR) technique is to extract the phase displacement component, while excluding residual phase components and especially noise. Although DInSAR enables the detection and quantification of land surface deformations with a precision in the order of millimeters [20], it does encounter several limitations and challenges; Spatio-temporal decorrelation [21] and atmospheric artifacts [22] are the two main restraints on the DInSAR technique leading to different errors of assessment. Permanent Scatterer Interferometry (PSI) [23] and Small BAseline Subset (SBAS) [24] have been developed to remove or mitigate the deficiencies of DInSAR. PSI is especially suited to the monitoring of urban areas—mainly consisting of man-made structures—as well as for vegetated regions using corner reflectors [25]. SBAS on the other hand, is primarily adapted for natural terrains, which lack an adequate number of PS pixels or may be partially covered by vegetation [26]. It is important to note that atmospheric artifacts cause phase delays in interferograms that can be generally mitigated through either phase-based methods, weather-oriented models [27] and GPS data [28].

Accordingly, the present study intends to use open-access SAR-S1 data with a medium resolution and revisit time of six days for post-war damage detection as an inexpensive tool for detecting building damages with no restrictions in terms of cloud cover and spectral resolution.

The proposed model uses SAR data to detect post-war damaged areas of Mosul, Iraq. Mosul, Iraq's second largest city, was overrun by ISIS on 4 June 2014 and was under exclusive control of ISIS for 29 months [29]. As collateral damage, the city's major civil

infrastructures were almost completely annihilated. The majority of destruction was made by the militant group ISIS, although airstrikes and military operations to recapture the city caused further damages as well. The amount of debris in the aftermath was estimated at 11 million tons [30], with the majority of damages inflicted upon the western sectors of Mosul (more than 90% destruction), particularly the Old City, with relatively limited damages seen in eastern Mosul [30]. The first steps mentioned towards the reconstruction of the area in the framework of the Mosul debris management program of the United Nation was to assess and clear the debris left as remnants of war. In the World Bank Report's assessment, the housing stock in Ninawa was most affected by the incursion, attributing 43% of the total share of reported damages to housing assets and the central urban area, which incurred 58% of the total damage (affected residential area: 2645 km$^2$). The estimated damage was 8001 billion Iraqi dinars [31]. The estimated figures demonstrate the need for an accurate, reliable and fast estimation of war-affected areas in the damage assessment procedure of any post-war reconstruction program. It should be noted that InSAR system is only capable of detecting displacement changes in order of few centimeters, depending on sensor wavelength between two successive acquisitions. Therefore, here we do not address the detection of the total destruction of a building, which can reach up to a vertical subsidence of several meters. Rather, we attempt to use InSAR as a tool to generally and relatively detect the extent of the war-affected areas. We hypothesize that the changes in vertical height of buildings caused by war can be associated with displacement changes detected using InSAR techniques to estimate damaged areas, of course, if no other displacement signals have contributed to the InSAR-based displacement estimation (e.g., land subsidence induced by groundwater depletion).

With the base premise of there being only one relevant study provided by UNITAR—a remote-based study to estimate inflicted damage using high-resolution images—that could be used to validate the results in this study, the present work offers findings of a novel, proposed assessment and analysis of post-war damage in Mosul using InSAR observations. To this end, SBAS, PSI and coherence-intensity-based change detection techniques have been applied to S1 data (2014–2017) to identify the post-war damage zones in Mosul. The results have been compared and validated with the UNITAR damage map of the city. This study will present a new insight into the capabilities of different InSAR-based techniques and take the advantage of S1 data to provide a fast, reliable, and cost-effective solution for initial urban damage estimation needed for post-war rehabilitation programs planning by decision-makers.

## 2. Materials and Methods

### 2.1. Study Area and Data

Mosul is a major city in the Ninawa Governorate of northern Iraq, located at the west bank of Tigris River. The metropolitan encompasses a relatively substantial territorial span on the left and right banks of the river, and is home to various ethnicities and religions. Mosul's population was estimated at 1,846,500 in 2014. From an economic perspective, the main products of the city include marble and oil. A detailed map of the city showing its main land uses and zonal division is presented in Figure 1A. In 2014, Mosul became the target of an incursion by ISIS, who seized control of the city, starting a humanitarian crisis which led to the internal displacement of 5 million Iraqis and occasioned the immense destruction of infrastructure and services. The government regained control after the Battle of Mosul in 2016–2017 although the city was heavily damaged during the recapture operation. Following the war, humanitarian aids initiated programs to provide emergency assistance for the rehabilitation and reconstruction of infrastructure and public facilities in Mosul. Numerous efforts were made, enabling conditions for the safe return of the displaced population to their homes. Estimation of damages was amongst other humanitarian endeavors in Mosul. At the close of war, the Iraqi Government requested the support of World Bank Group (WBG) to undertake a Damage and Needs Assessment (DNA) with the aim of estimating the effects and impacts

of the crisis on key infrastructure as well as service delivery, livelihood, social wellbeing, productivity, and cross-cutting sectors, and to identify recovery and reconstruction needs in Iraq [31]. Accordingly, a multi-disciplinary team formed by members of UN-Habitat and UNESCO was tasked with developing an initial planning framework for the reconstruction of Mosul with the support of the local government [32]. The proposed undertaking included the use of drone imagery, satellite images and field visits to create a post-war damage map. The findings revealed that a total of 1690, 3241, and 9455 buildings were damaged and categorized as destroyed, with severe and negligible damage within the Old City [32]. In another estimation performed by the UNITAR–UNOSAT, they identified a total of 19,888 affected structures within the city. Approximately 4773 of these were destroyed, 8233 severely damaged and 6882 moderately (Figure 1B) damaged. As the generated map (UNITAR) shows, the majority of damages occurred in the western sectors of Mosul with the most severe damage sustained in the Old City. The proposed map shows severely and moderately damaged and completely destroyed buildings identified by optical satellite imagery.

### 2.2. SBAS- and PSI-Based Deformation Detection

SARscape® (Switzerland) was used to process S1-A/B data in order to measure the amount of deformation using SBAS, PSI, and coherence-intensity-based change detection techniques, for the post-war damage assessment of Mosul city.

The following steps were taken in the SBAS processing phase [24] (Figure 2): (1) creation of connection graphs using temporal (one month) and spatial baseline (20% of the critical baseline of S1 data (i.e., 5 km)) thresholds for each sensor; the critical baseline is the distance between two satellite passes that if exceeded results in a complete loss of coherence in the interferograms; (2) interferometric processing by the registering of slave images to master image in order to generate interferograms; the process included the calculation of a local nonparametric shift estimate using DEM and orbital information incorporated with the application of a set of windows ($64 \times 64$ in range and $128 \times 128$ in azimuth) on the master image to compute the cross-correlation function. To increase the signal-to-noise ratio of the interferograms for a more reliable coherence estimation, a multi-looking factor of $4 \times 1$ was applied (i.e., pixel size of ~14 m $\times$ 14 m on the ground from the original pixel spacing of $2.3 \times 13.9$ m). The Goldstein filter was also assigned on the interferograms and the Minimum Cost Flow method was employed for unwrapping [33]; (3) re-flatting and refinement of unwrapped interferograms using a third-degree polynomial to remove ramps (orbital errors) and constant phase offset; (4) first phase of inversion for the estimation of initial ground deformation following the removal of height residual (due to DEM error); (5) second phase of inversion for the removal of atmospheric artefacts by assigning a two dimensional spatial low-pass filter and a temporal high-pass filter to estimate final ground deformation; and (6) georeferencing of final deformations map.
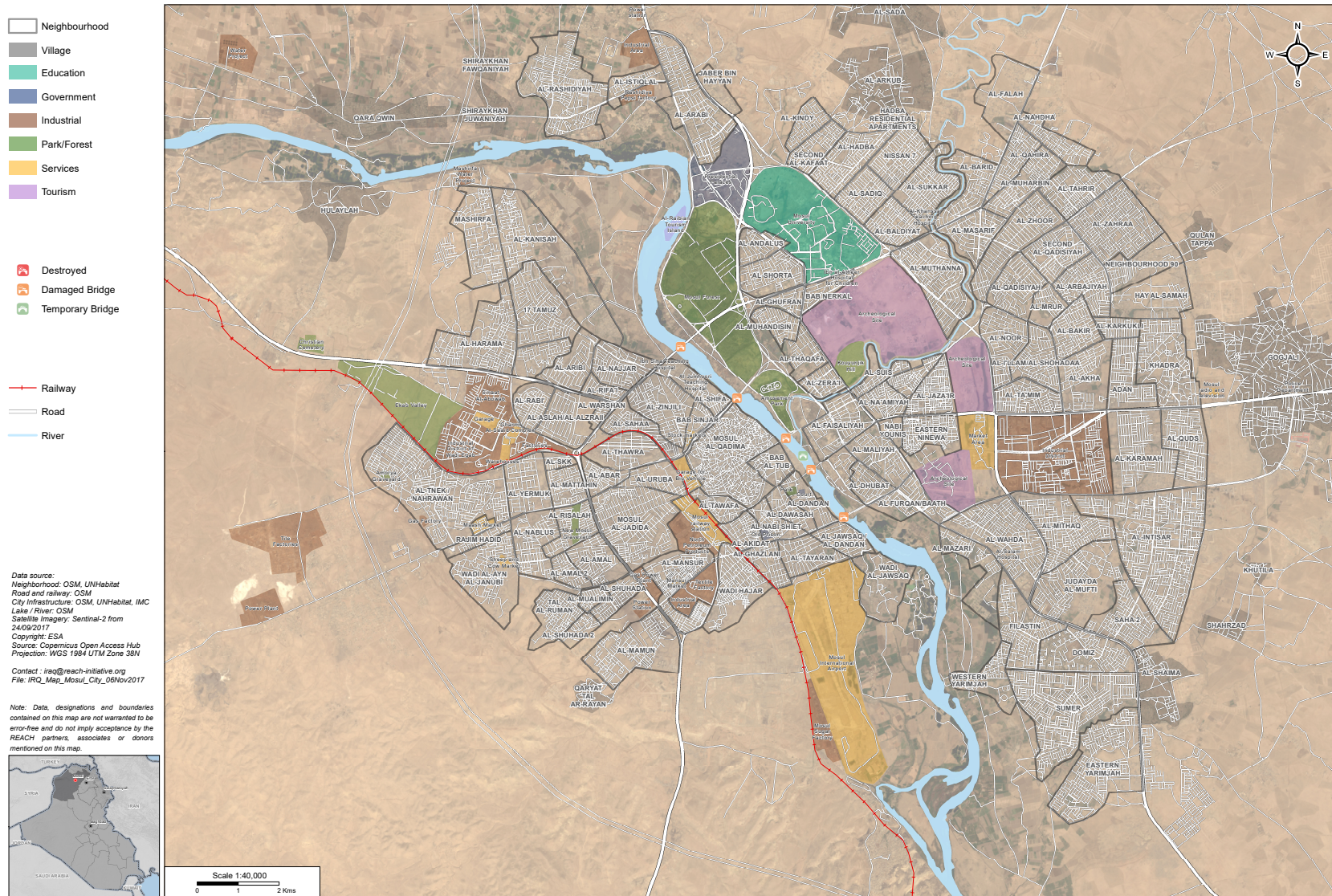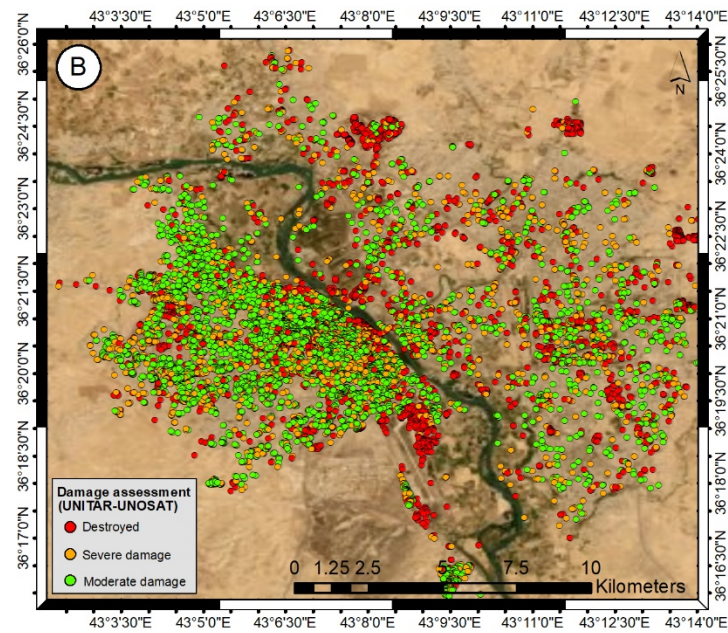
**Figure 1.** *Cont.*

**Figure 1.** Map of Mosul and estimated damaged buildings. (**A**) shows zonal division and major land uses (data source: UNHabitat, 2019) and (**B**) shows three classes of damage severity in colored dots, courtesy of UNITAR-UNOSAT. The source for the UNITAR-UNOSAT map is available at: http://unosat-maps.web.cern.ch/unosat-maps/IQ/CE20140613IRQ/UNOSAT_A3_Mosul_damage_assessment_4August2017_Landscape2_o.pdf (accessed date: 15 November 2020)
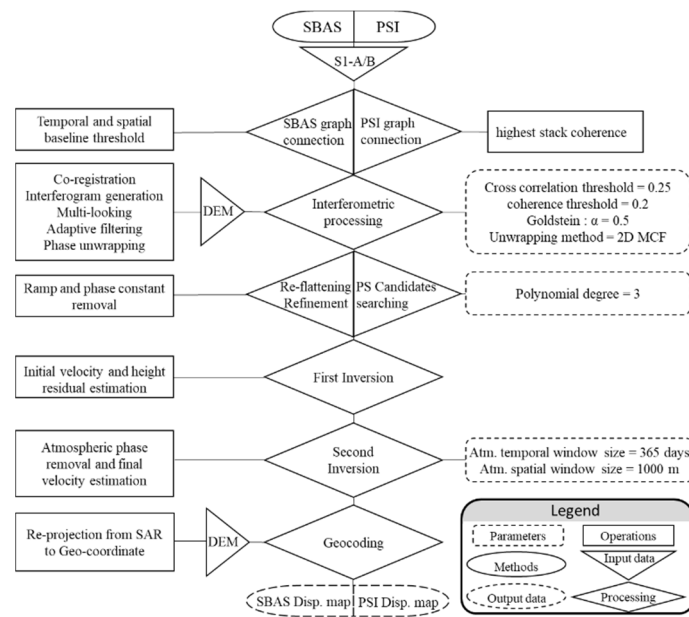
**Figure 2.** Workflow of the Small BAseline Subset (SBAS) and Permanent Scatterer Interferometry (PSI) processing in six steps.

The steps in PSI processing [34] were similar to SBAS processing with the following distinctions in PSI: (1) the connection graph is a star-like graph and the master image is selected based on the highest stack coherence adopted for the S1 data to maximize the sum correlation of all interferograms [25], and (2) in the PS candidate searching step, the initial PSs are selected based on the dispersion index [34] as a proxy for phase stability, and in the re-flattening and refinement steps, several coherent pixels (>0.9) with movement rates of zero were selected for the constant phase offset removal (Figure 2).

### 2.3. Coherence-Based Change Detection

Local coherence ($\hat{\gamma}$) represents the complex cross-correlation coefficient of a SAR image pair ($u_{1i}, u_{2i}$) estimated using $N$ independent image samples over a small window of the size-range 0 (the interferometric phase is only noise) to 1 (complete absence of phase noise):

$$\hat{\gamma} = \frac{\sum_{i=1}^{N} u_{1i} u_{2i}^*}{\sqrt{\sum_{i=1}^{N} |u_{1i}|^2} \sqrt{\sum_{i=1}^{N} |u_{2i}|^2}} \tag{1}$$

### 3. Results

### 3.1. DInSAR City Monitoring (SBAS–PSI)

Results of SBAS and PSI processing for Mosul are presented in Figure 3. The four rectangles in the displacement maps in Figure 3A illustrate examples of the destructed areas, indicating an increase in distance between the satellite and buildings (blue and purple colors). The rectangles include areas selected to be checked on the high-resolution optical imageries (30 cm) of the WorldView-3 (VNIR) taken from Digital Glob. Pixels with negative values in the SBAS and PSI displacement map could be associated with ruined regions including destroyed buildings. The color range in the corner of each map indicates the severity of destruction, with the blue and purple range of color implying higher severity (greater increase in the distance between the satellite and urban infrastructures). As evident in the resultant maps, the highest volume of destruction occurred in the area encompassed by rectangle "c" (purple colors), corresponding to the Old City of Mosul. A comparison of regions identified as damaged areas (enclosed within the three rectangles) on maps (Figure 3A,B) with optical images taken before and after the ISIS incursion and

subsequent war shows the accuracy of areas marked by negative values in the SBAS and PSI displacement maps as damaged regions.
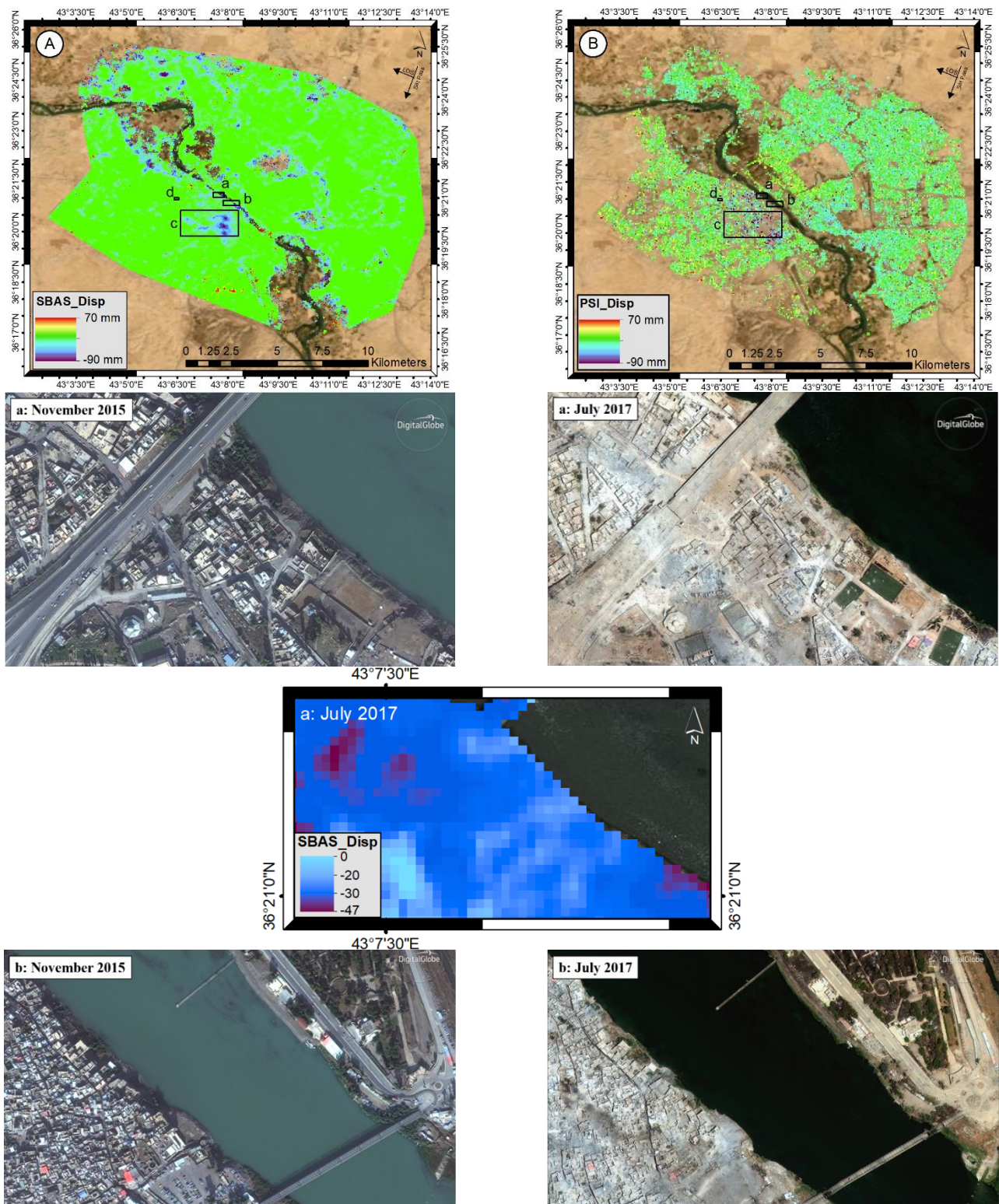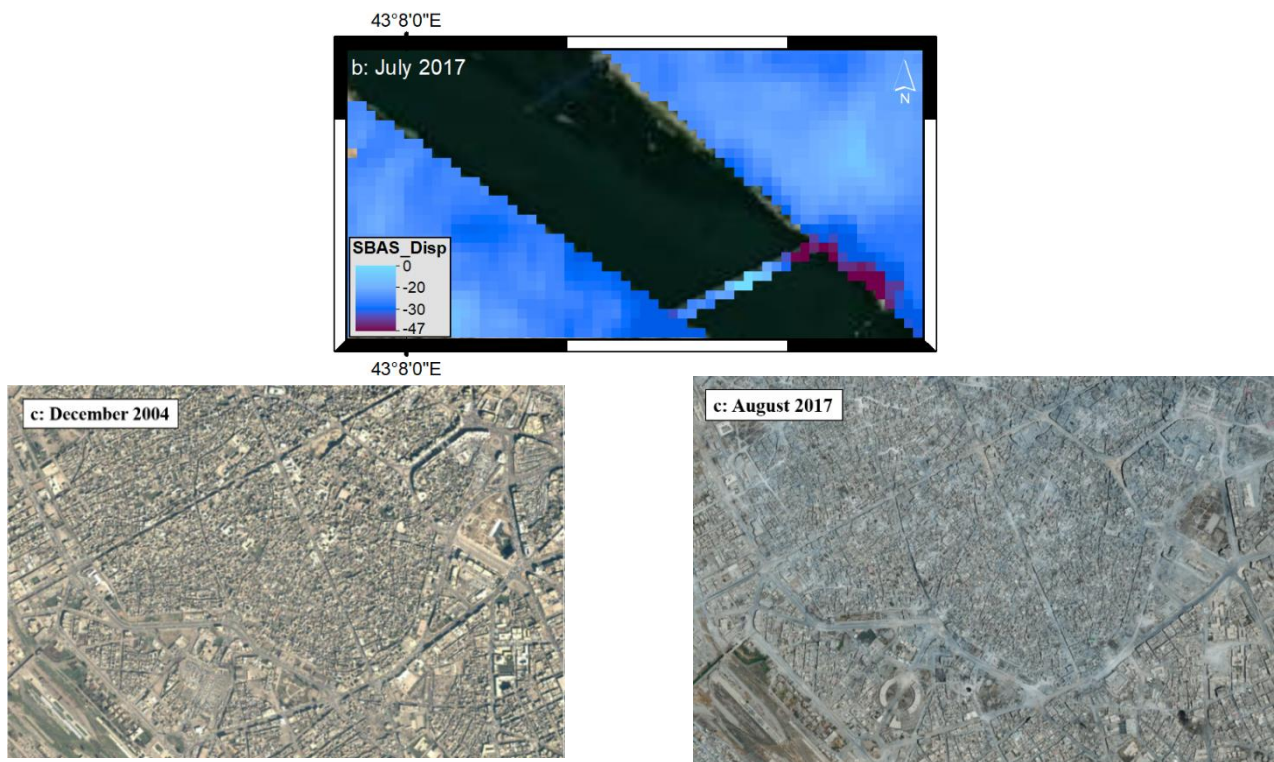


**Figure 3.** *Cont.*

**Figure 3.** Results of SBAS and PSI damage assessment for Mosul. (**A**) SBAS displacement map and (**B**) PSI displacement map. Positive (negative) values indicate a decrease (increase) in the distance between satellite and objects on the ground. Below the displacement maps are the WorldView-3 (VNIR) high resolution images taken from DigitalGlobe for the purpose of visual comparison of estimated damages in the three selected rectangles. The corresponding zones of "a", "b" and "c" of SBAS displacement map have also been displayed.

We here analyzed several samples of displacement time-series to investigate the correspondence between abrupt SBAS-displacements and the dates coinciding with, e.g., war operations, bombings, or other events. The results are then compared with the UNITAR maps. The analysis initially begins with the Old City area (Figure 4A: zoomed rectangular "c" in Figure 3A), which sustained the most damage as the collateral of war, especially during the recapture operation of Mosul. For this purpose, five pixels were selected as samples (i.e., a, b, c, d, and e), each corresponding to areas which seemingly received serious damages (Figure 4A). The UNITAR points of the destroyed buildings were than overlaid on the SBAS displacements map (Figure 4B). As the results suggest, the displacement time-series extracted for the five selected points show similar trends in damage to that of the UNITAR, with differences in magnitude (Figure 4C). Figure 4C also depicts different phases of the military operations launched to liberate the city (Battle of Mosul, 2016–2017), including (1) phase one (October–December 2016); (2) phase two (December 2016–February 2017); and (3) phase three (February–July 2017) shown in purple, green and pink, respectively. During the first phase, international coalition forces started entering the city from the east, advancing towards the Syrian border. Phase two consisted of the recapture of eastern Mosul on January 2017. The city was then fully retaken as part of phase three on July 2017, albeit many post-victory clashes prolonged to 2018.
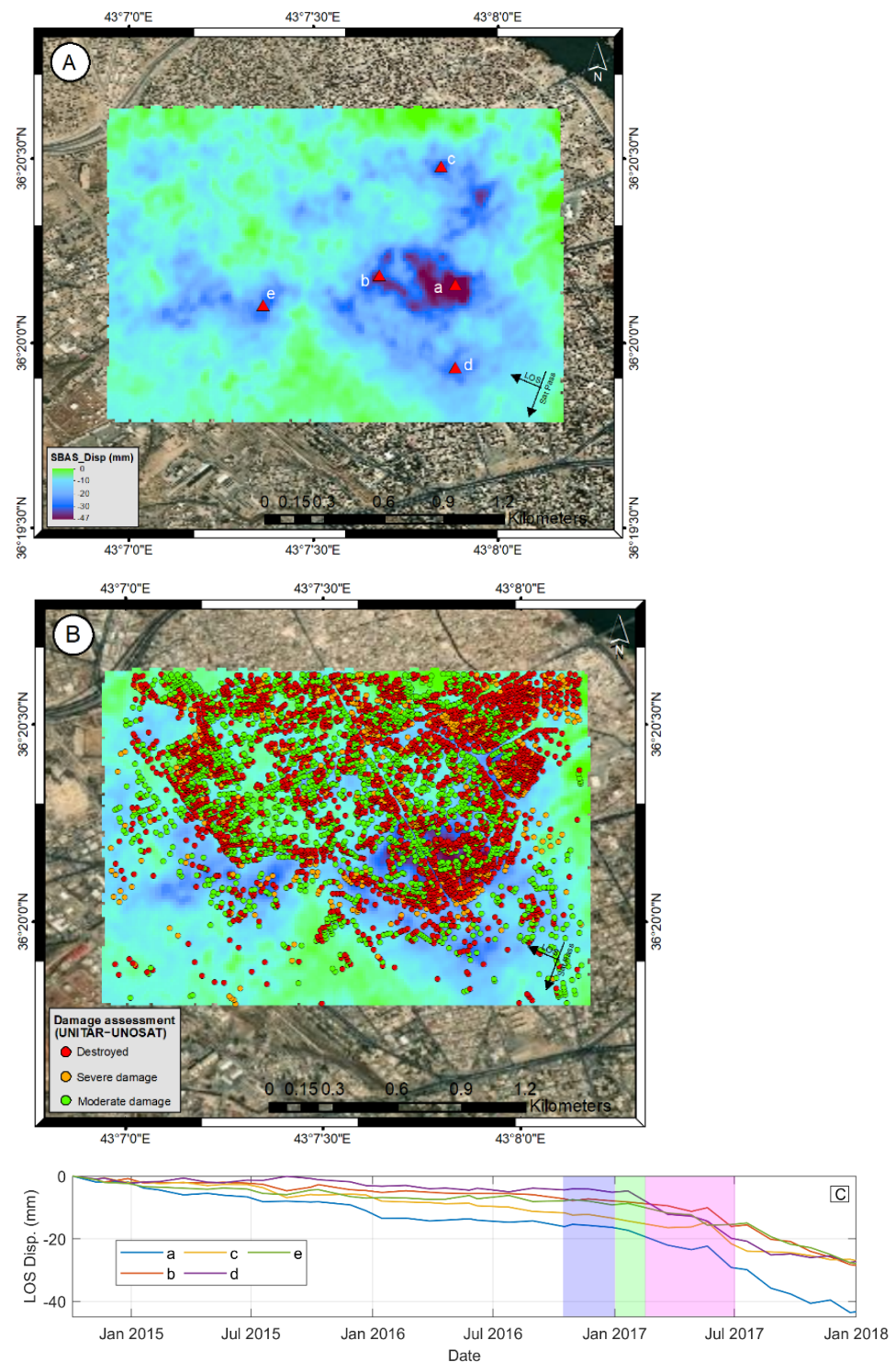
**Figure 4.** Trends in SBAS-displacement and their relation to war events. (**A**) Zoomed view of rectangle "c" on Figure 3A with five selected points. (**B**) The damaged buildings detected by the UNITAR-UNOSAT classified as the destroyed buildings (red points) superimposed over the SBAS-displacement map. The SBAS pixels with no corresponding red points have been masked. (**C**) SBAS-displacement time series images of the selected points on Figure 4A plotted along with the time-span of the three phases of the recapture operation of Mosul; phase 1 (purple), phase 2 (green), and phase 3 (pink). Further information on the timeline of the retake operation of Mosul can be found in Battle of Mosul on Wikipedia.

The aftermath brought on by the use of heavy ground weapons such as artilleries and airstrikes in the Mosul battles brought immense destruction to residential areas and urban infrastructures. As can be seen from Figure 4C, the displacement time-series show three distinctive trends of damage: slight increase (less changes/damages) from the time the city was seized by ISIS to before the first phase of the recapture operation; and intense increase (intense changes/damages) from the beginning of the first phase of the recapture operation through 2018. The deceasing trend observed in the time-series displacements are in consonance with the three phases of the recapture operation. Raster pixels in the SBAS displacement map, corresponding to red points (destroyed buildings), have mostly negative values, indicative of the damaged residential areas in the SBAS map (Figure 4B).

During the next steps of analysis, the obtained SBAS results were compared with the three different damage classes provided by UNITAR (i.e., moderate, severe damage, and destroyed). The comparison was made for the Al-Shafaa district in Mosul, which sustained the most damage after the Old City (Figure 5A: zoomed rectangular "d" in Figure 3A). Two images of the Al-Shafaa district are depicted in this study, the first is a WorldView-3 Imagery taken in 18 February 2017 with the pixel size of 40 cm (Figure 5A) and the second is a GeoEye-1 Imagery taken in 4 August 2017 with the pixel size of 50 cm (Figure 5B). The status of healthy and damaged buildings is clearly observable in both high-resolution images. The SBAS displacement map, corresponding to Figure 5A,B, has been presented along with the three classes of the UNITAR points (Figure 5C). Fifty-five points are seen overlaid over the post-war image (Figure 5B), showing the severity of damages categorized as moderate damage (green points), severe damage (orange points), and destroyed buildings (red points). Several conclusions can be drawn by superimposing the UNITAR points over the SBAS displacement map. All SBAS pixels corresponding to the UNITAR points have negative values (an increase in distance between satellite and objects on the ground) implying that SBAS is generally successful in detecting damaged buildings. In some cases, the red and orange points located over the purple (pixel value between −23 mm and −47 mm) and dark blue (between −20 mm and −30 mm) pixels suggest that more severe damages led to more negative values, albeit this is not the case for all points. The finding could be used as an indicator of the feasibility and efficiency of employing InSAR, particularly high-resolution SAR images, for damage assessment of buildings. We here used the UNITAR data as the ground truth to evaluate the accuracy of the SBAS result. Both results could be also considered as two complementary pieces of information. On one hand UNITAR provides pointwise information over damage of each single building in details, but on the other hand SBAS presents a dense map of changes associated with the urban damages not only limited to the buildings but also include damages to other urban infrastructures such as streets. As a result, integration of both information could bring us more precise and comprehensive estimation of the extent and degree of the war-affected areas.
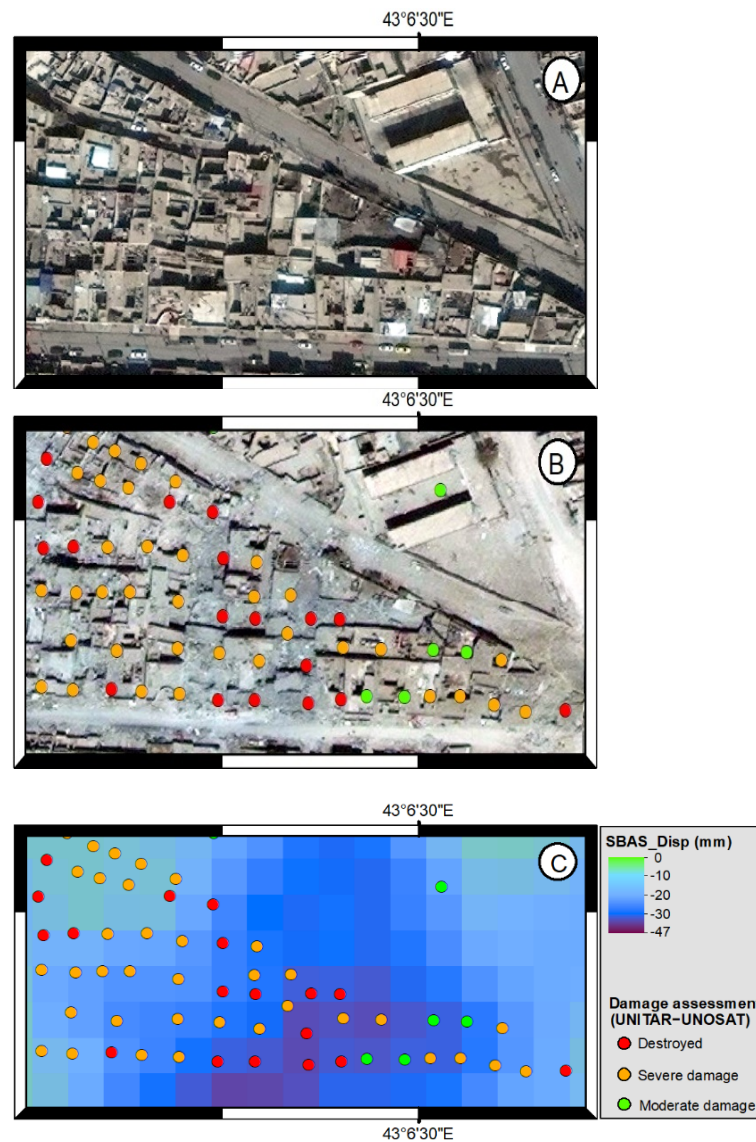
**Figure 5.** Cross comparison of the UNITAR result with the SBAS displacement map. (**A**) WorldView-3 Imagery (18 February 2017) and (**B**) GeoEye-1 Imagery (4 August 2017) of the Al-Shafaa district (Copyright: DigitalGlobe, Inc. and Source: Department of State, Humanitarian Information Unit, NextView License). (**C**) SBAS displacement map with three classes of damaged severity shown in colored dots, courtesy of UNITAR-UNOSAT. The source for the UNITAR-UNOSAT map is available at: http://unosat-maps.web.cern.ch/unosat-maps/IQ/CE20140613IRQ/UNOSAT_A3_Mosul_damage_assessment_4August2017_Landscape2_o.pdf (accessed date: 15 November 2020).

*3.2. Coherence-Based Change Detection*

The coherency map of Mosul city, calculated between first and second S1 data (Figure 6A), corresponding to the 4 October and 9 November 2014 (pre-war period), was used to obtain an overall profile of the city's damage status before the ISIS takeover. Another coherency map, calculated between the first and last (35th: 25 August 2017) images, was used to detect changes in urban infrastructures as the result of war (Figure 6B). The distinctions between the two coherency maps are clearly tangible and visually interpretable. Regions with high coherency values (dark blue areas in Figure 6A) appear to fade out and lose coherency in the direction of the left bank of the river (light blue areas in Figure 6B). As an additional step, intensity information (average of the backscatter) of the S1 data was used to generate an RGB color composite for the visualization and identification of coherent temporal changes. Figure 6C,D have been produced using the first and second S1 data in

the pre-war period and the first and 35th S1 data in post-war period, respectively. In both maps, master and salve intensities are shown respectively in red and green bands, with coherency assigned to the blue band (called hereafter MAC). In the MAC maps, the color combinations confirm that the most important changes have been identified by variations in coherence. In the pre-war MAC map (Figure 6C), the color yellow is used to indicate only similar master-slave intensity, and white is used to indicate similar master-slave intensity and high coherency. In the post-war MAC map (Figure 6D), the loss of coherency (blue color) is clearly observed and the superiority of yellow-green color manifests itself particularly in the western bank of the river (Old City). The yellow color in the post-war MAC is an indication of the same master and slave intensity, corresponding to low coherence regions. The higher frequency of green pixels as opposed to yellow ones demonstrates that the backscattering of destroyed regions on the slave image has increased (referring to volume scattering mechanism). Red color pixels represent regions where the backscattering on the master image was higher than on the slave image. The red pixels are mainly related to agricultural lands and certain areas with low coherency that were destroyed after the war.
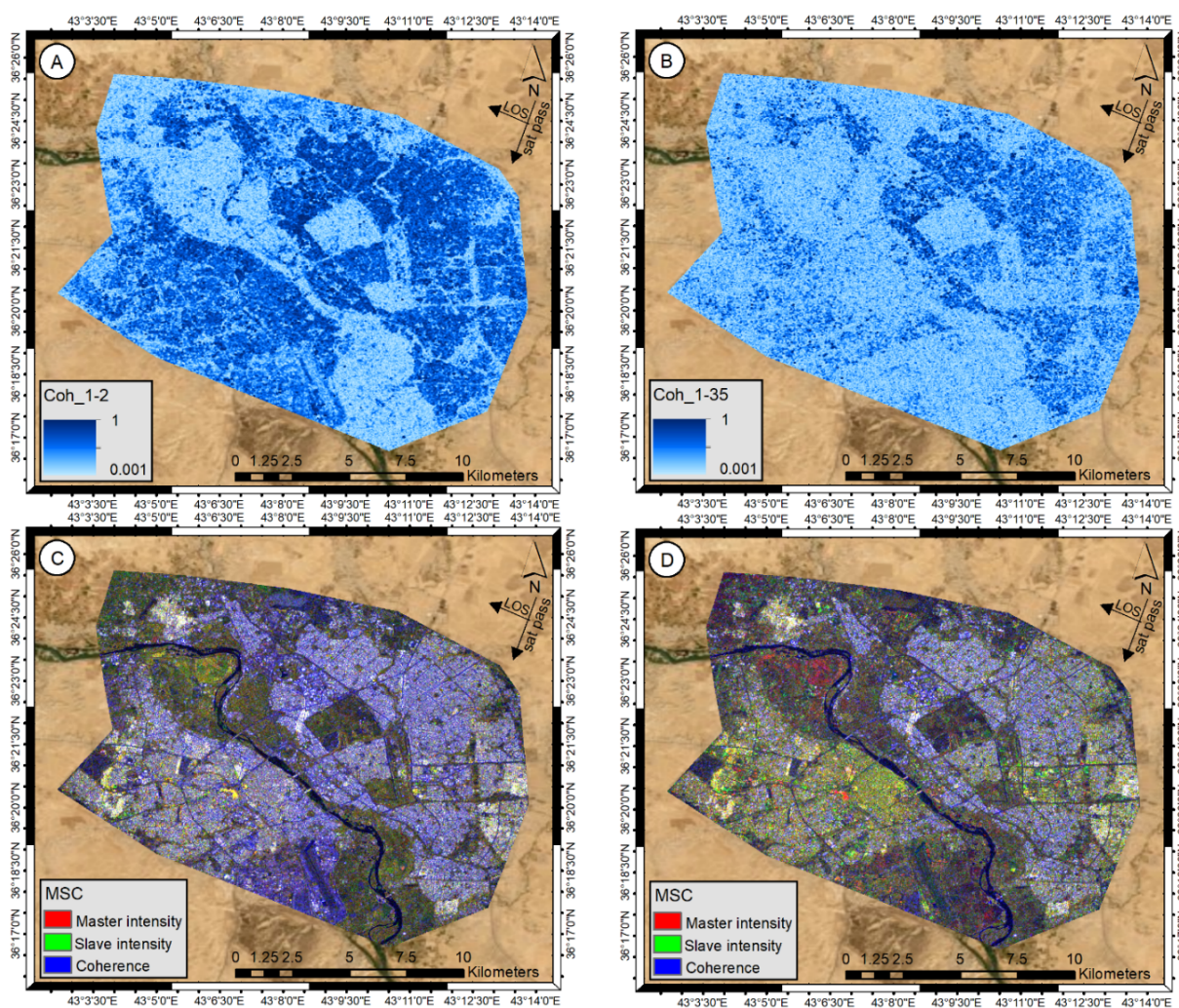


**Figure 6.** Coherence and intensity maps. (**A**) the coherence map estimated using the first and second S1 data (pre-war period), (**B**) the coherence map estimated using the first and last (35th) S1 data (post-war period), (**C**) RGB color composite of Master–Agent intensity and Coherency (MAC) obtained by using the first and second S1 data (pre-war period) and (**D**) MAC estimated using the first and last (35th) S1 data (post-war period).

In order to bypass changes in non-urban areas, all regions with coherence values lower than 0.3 (mainly related to vegetated areas, farmlands and bare soil) were masked in the coherence change detection phase to ensure that only changes of high coherent objects such as buildings contributed to the coherence analysis. Firstly, the coherence map between the first and second images in the time-series set of images was generated as a reference map of healthy urban infrastructures (Figure 7C). In the second place, the coherence map between the first and last images was generated and regions with coherency reduction and loss were extracted as damaged areas of war. The obtained map was then compared with Figure 7C in a pixel-by-pixel fashion. The coherence value of pixels showing a considerable reduction were considered as war-affected areas (see Figure 7D).
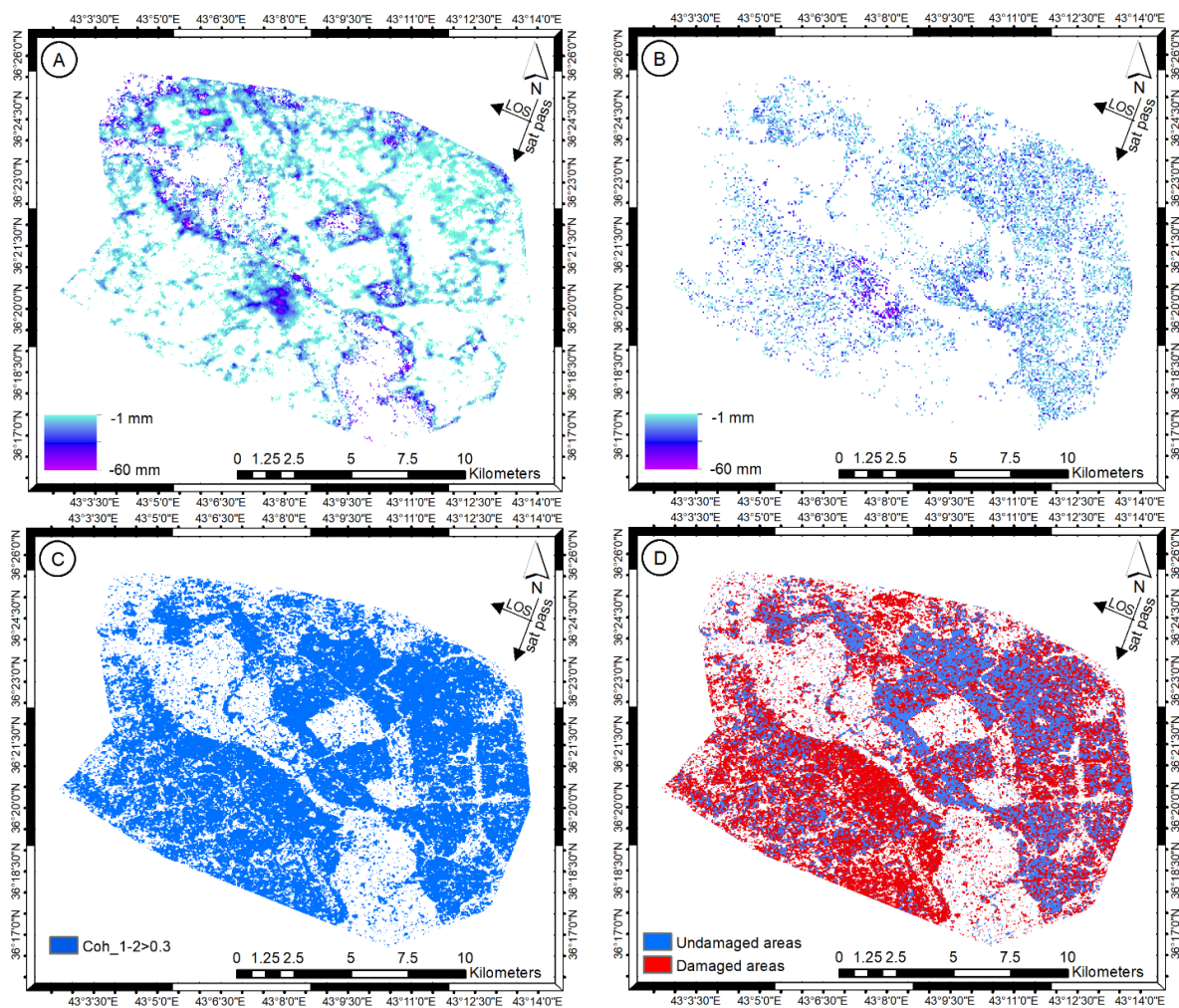


**Figure 7.** Estimation of damaged regions in Mosul. (**A**) SBAS and (**B**) PSI displacement maps masked for pixel values higher than −1; (**C**) Coherence-masked map calculated between the first and second images masked for pixel values lower than 0.3, indicating man-made structures and (**D**) damaged and undamaged areas extracted from the coherency map estimated from images at positions 1–2 and 1–35.

## 4. Discussion

War-affected areas could be identified with the underlying assumption that negative values in the SBAS and PSI displacement map correspond to an increase in the distance between satellite and objects on the ground, and associated with destroyed urban infrastructures. Of course, other factors may influence the displacement values derived by PSI-SABS such as contribution of phase changes induced by probable land subsidence due to overexploitation of ground water. Nevertheless, the possibility of the presence of

such factors was ignored for the study area, as no related evidence has been reported for the city of Mosul. Accordingly, the destruction map of the city was made by masking values higher than $-1$ mm in the PSI–SABS displacement maps to ensure that an increase between satellite and buildings is considered. These masked values correspond to decreases in height of buildings due to destruction. As such, the war-induced destructions in urban structures could be detected by accounting for temporal changes in the pre- and post-war coherency maps. Of course, the entire changes in height of buildings caused by war, reaching a few meters at most, cannot be detected by InSAR techniques given the half-wavelength limitation of the SAR system to estimate displacements between two consecutive acquisitions. Hence, only part of the real reduction in height of buildings can be captured by InSAR. The final masked PSI–SBAS displacement maps have been provided in Figure 7A,B.

The final results were evaluated against damaged map of the Mosul city (UNITAR), created using high-resolution optical imagery including, GeoEye-1 (4 August 2017), WorldView-3 (8 February 2017), and WorldView-2 (15 November 2013) (Figure 1B). Based on the findings of this study, a total of 19,888 affected structures were identified within the city, of which an approximate 4773 were destroyed, 8233 severely damaged, and 6882 moderately damaged. Around 7620 of cases occurred within the Old City of Mosul.

Results from the SBAS-PSI displacement and coherence-based change detection maps agree with the UNITAR map, in terms of identified damaged regions, especially in the old city. Nevertheless, the PSI map provided a denser point-wise map of the city (130,075 points) compared to the "UNITAR" map (20,787 points). The difference in PS pixels was mainly attributable to buildings and other man-made urban infrastructures. While the damaged map obtained by the coherence analysis (Figure 7D) presents a high agreement with the UNITAR map, the severity and extent of damages were estimated at much higher rates. The coherence changes detected between the first and last images show the war-damage, expanding to 65,450 km$^2$ in size or nearly 40% of the urban area of Mosul.

Although the UNITAR maps were used for cross comparison, the lack of accurate ground data such as building height has made it difficult for linking LOS InSAR displacement with the amount of building damages incurred. One shortcoming of the medium-spatial resolution S1 data is its incapacity to map urban damage at the building scale. Using high-resolution SAR data, such as TerraSAR-X, with different polarizations, would provide further information on each damaged building.

## 5. Conclusions

This study presented an analysis of post-war-affected areas of Mosul City using S1 data. The proposed methodology used SBAS, PSI systems along with coherence- and intensity-based change detection techniques to map the destroyed zones. The results showed that 40% of the city's infrastructure is affected by the collateral damage of war. Compared with the previous damage assessment map provided by UNITAR, it seems that the UNITAR map of damaged buildings is an underestimation of the actual zones destroyed and the extent of war-damaged areas in the city. One reason for this underestimation could be related to the fact that the UNITAR considered only the damaged residential buildings and urban infrastructure while coherence analysis detected the damages to all kinds of man-made structures (coherence > 0.3) in the city. This study showed that S1 data, especially coherence change detection, can be generally used to detect war-induced damages and can be used as a robust tool to provide reliable information for decision-makers to plan post-war reconstruction programs or other disaster control procedures.

Despite the lack of distinction between different types of damages (e.g., slight, moderate, and severe damage), due to the fact that a sudden decrease in building height cannot be detected by InSAR (half-wavelength limitation), the study showed that it is possible to link building height variations with changes in coherence values to create an empirical model for determining damage severity, provided that ground data is available. This could be an issue to be followed in future research.

## References

1. Ruiz-Armenteros, A.M.; Lazecky, M.; Hlaváčová, I.; Bakoň, M.; Manuel Delgado, J.; Sousa, J.J.; Lamas-Fernández, F.; Marchamalo, M.; Caro-Cuenca, M.; Papco, J.; et al. Deformation monitoring of dam infrastructures via spaceborne MT-InSAR. The case of La Viñuela (Málaga, southern Spain). *Procedia Comput. Sci.* **2018**, *138*, 346–353. [CrossRef]
2. Mishra, B.; Susaki, J. Optical and SAR data integration for automatic change pattern detection. *ISPRS Ann. Photogramm. Remote Sens. Spat. Inf. Sci.* **2014**, *II*, 39–46. [CrossRef]
3. Stramondo, S.; Bignami, C.; Pierdicca, N.; Chini, M. SAR and optical remote sensing for urban damage detection and mapping: Case studies. *2007 Urban Remote Sens. Jt. Event URS* **2007**, 1–6. [CrossRef]
4. Noviello, C.; Verde, S.; Zamparelli, V.; Fornaro, G.; Pauciullo, A.; Reale, D.; Nicodemo, G.; Ferlisi, S.; Gullà, G.; Peduto, D. Monitoring buildings at landslide risk with SAR: A methodology based on the use of multipass interferometric data. *IEEE Geosci. Remote. Sens. Mag.* **2020**, *8*, 91–119. [CrossRef]
5. Chini, M.; Pierdicca, N.; Emery, W.J. Exploiting SAR and VHR optical images to quantify damage caused by the 2003 Bam earthquake. *IEEE Trans. Geosci. Remote Sens.* **2008**, *47*, 145–152. [CrossRef]
6. Moro, M.; Saroli, M.; Stramondo, S.; Bignami, C.; Albano, M.; Falcucci, E.; Gori, S.; Doglioni, C.; Polcari, M.; Tallini, M.; et al. New insights into earthquake precursors from InSAR. *Sci. Rep.* **2017**, *7*, 1–11. [CrossRef]
7. Lubin, A.; Saleem, A. Remote sensing-based mapping of the destruction to Aleppo during the Syrian Civil War between 2011 and 2017. *Appl. Geogr.* **2019**, *108*, 30–38. [CrossRef]
8. Li, Q.; Gong, L.; Zhang, J. A correlation change detection method integrating PCA and multi-texture features of SAR image for building damage detection. *Eur. J. Remote Sens.* **2019**, *52*, 435–447. [CrossRef]
9. Nex, F.; Duarte, D.; Tonolo, F.G.; Kerle, N. Structural building damage detection with deep learning: Assessment of a state-of-the-art cnn in operational conditions. *Remote Sens.* **2019**, *11*, 2765. [CrossRef]
10. Park, S.-E.; Jung, Y.T. Detection of Earthquake-Induced Building Damages Using Polarimetric SAR Data. *Remote Sens.* **2020**, *12*, 137. [CrossRef]
11. Poulain, V.; Inglada, J.; Spigai, M.; Tourneret, J.-Y.; Marthon, P. High-resolution optical and SAR image fusion for building database updating. *IEEE Trans. Geosci. Remote Sens.* **2011**, *49*, 2900–2910. [CrossRef]
12. Dong, L.; Shan, J. A comprehensive review of earthquake-induced building damage detection with remote sensing techniques. *ISPRS J. Photogramm. Remote Sens.* **2013**, *84*, 85–99. [CrossRef]
13. Gillespie, T.W.; Chu, J.; Frankenberg, E.; Thomas, D. Assessment and prediction of natural hazards from satellite imagery. *Prog. Phys. Geogr.* **2007**, *31*, 459–470. [CrossRef]
14. Washaya, P.; Balz, T.; Mohamadi, B. Coherence change-detection with Sentinel-1 for natural and anthropogenic disaster monitoring in urban areas. *Remote Sens.* **2018**, *10*, 1026. [CrossRef]
15. Ghandour, A.; Jezzini, A. Post-War Building Damage Detection. *Proceedings* **2018**, *2*, 359. [CrossRef]
16. Matsuoka, M.; Yamazaki, F. Characteristics of satellite SAR images in the areas damaged by earthquakes. In Proceedings of the IEEE 2000 International Geoscience and Remote Sensing Symposium. Taking the Pulse of the Planet: The Role of Remote Sensing in Managing the Environment. (Cat. No. 00CH37120), Elizabeth City, NC, USA, 24–28 July 2000; Volume 6, pp. 2693–2696. [CrossRef]
17. Hosokawa, M.; Jeong, B.; Takizawa, O. Earthquake damage detection using remote sensing data. In Proceedings of the 2007 IEEE International Geoscience and Remote Sensing Symposium, Barcelona, Spain, 23–27 July 2007; pp. 2989–2991.
18. Yonezawa, C.; Takeuchi, S. Decorrelation of SAR data by urban damages caused by the 1995 Hyogoken-nanbu earthquake. *Int. J. Remote Sens.* **2001**, *22*, 1585–1600. [CrossRef]
19. Yonezawa, C.; Tomiyama, N.; Takeuchi, S. Urban damage detection using decorrelation of SAR interferometric data. In Proceedings of the IEEE International Geoscience and Remote Sensing Symposium, Toronto, ON, Canada, 24–28 June 2002; Volume 4, pp. 2051–2053.
20. Bamler, R.; Hartl, P. Synthetic aperture radar interferometry. *Inverse Probl.* **1998**, *14*, 55. [CrossRef]

21. Zebker, H.A.; Villasenor, J. Decorrelation in interferometric radar echoes. *IEEE Trans. Geosci. Remote Sens.* **1992**, *30*, 950–959. [CrossRef]

22. Zebker, H.A.; Rosen, P.A.; Hensley, S. Atmospheric effects in interferometric synthetic aperture radar surface deformation and topographic maps. *J. Geophys. Res. Solid Earth* **1997**, *102*, 7547–7563. [CrossRef]

23. Ferretti, A.; Prati, C.; Rocca, F. Permanent scatterers in SAR interferometry. *IEEE Trans. Geosci. Remote. Sens.* **2001**, *39*, 8–20. [CrossRef]

24. Berardino, P.; Fornaro, G.; Lanari, R.; Sansosti, E. A new algorithm for surface deformation monitoring based on small baseline differential SAR interferograms. *IEEE Trans. Geosci. Remote Sens.* **2002**, *40*, 2375–2383. [CrossRef]

25. Darvishi, M.; Schlögel, R.; Bruzzone, L.; Cuozzo, G. Integration of PSI, MAI, and intensity-based sub-pixel offset tracking results for landslide monitoring with X-band corner reflectors-Italian Alps (Corvara). *Remote Sens.* **2018**, *10*, 409. [CrossRef]

26. Darvishi, M.; Schlögel, R.; Kofler, C.; Cuozzo, G.; Rutzinger, M.; Zieher, T.; Toschi, I.; Remondino, F.; Mejia-Aguilar, A.; Thiebes, B.; et al. Sentinel-1 and Ground-Based Sensors for Continuous Monitoring of the Corvara Landslide (South Tyrol, Italy). *Remote Sens.* **2018**, *10*, 1781. [CrossRef]

27. Darvishi, M.; Cuozzo, G.; Bruzzone, L.; Nilfouroushan, F. Performance evaluation of phase and weather-based models in atmospheric correction with Sentinel-1data: Corvara landslide in the Alps. *IEEE J. Sel. Top. Appl. Earth Obs. Remote Sens.* **2020**, *13*, 1332–1346. [CrossRef]

28. Fornaro, G.; D'Agostino, N.; Giuliani, R.; Noviello, C.; Reale, D.; Verde, S. Assimilation of GPS-derived atmospheric propagation delay in DInSAR data processing. *IEEE J. Sel. Top. Appl. Earth Obs. Remote Sens.* **2014**, *8*, 784–799. [CrossRef]

29. Lafta, R.; Al-Nuaimi, M.A.; Burnham, G. Injury and death during the ISIS occupation of Mosul and its liberation: Results from a 40-cluster household survey. *PLoS Med.* **2018**, *15*, 1–20. [CrossRef]

30. United Nations Environment Programme. *Environmental Issues in Areas Retaken From Isil Mosul, Iraq Rapid Scoping Mission*; UNEP: Nairobi, Kenya, 2017.

31. World Bank. *Iraq Reconstruction and Investment*; Part 2; World Bank: Washington, DC, USA, 2018.

32. Habitat for Humanity. *Initial Planning Framework for the Reconstruction of Mosul*; HH: Atlanta, GA, USA, 2018.

33. Pepe, A.; Lanari, R. On the Extension of the Minimum Cost Flow Algorithm for Phase Unwrapping of Multitemporal Differential SAR Interferograms. *IEEE Trans. Geosci. Remote Sens.* **2006**, *44*, 2374–2383. [CrossRef]

34. Ferreti, A.; Prati, C.; Rocca, F. Nonlinear subsidence rate estimation using permanent scatterers in differential SAR interferometry. *IEEE Trans. Geosci. Remote Sens.* **2000**, *38*, 2202–2212. [CrossRef]